HHS Public Access

Author manuscript

Cell Rep. Author manuscript; available in PMC 2022 September 06.

Published in final edited form as:

Cell Rep. 2022 August 16; 40(7): 111203. doi:10.1016/j.celrep.2022.111203.

STK25 inhibits PKA signaling by phosphorylating PRKAR1A

Xiaokan Zhang[1], **Bryan Z. Wang**[1,2], **Michael Kim**[1], **Trevor R. Nash**[1,2], **Bohao Liu**[1,2], **Jenny Rao**[1], **Roberta Lock**[2], **Manuel Tamargo**[2], **Rajesh Kumar Soni**[3], **John Belov**[1], **Eric Li**[1], **Gordana Vunjak-Novakovic**[1,2], **Barry Fine**[1,4,*]

[1]Department of Medicine, Division of Cardiology, Columbia University Irving Medical Center, New York, NY 10032, USA

[2]Department of Biomedical Engineering, Columbia University, New York, NY, USA

[3]Proteomics and Macromolecular Crystallography Shared Resource, Herbert Irving Comprehensive Cancer Center, Columbia University Irving Medical Center, New York, NY, USA

[4]Lead contact

SUMMARY

In the heart, protein kinase A (PKA) is critical for activating calcium handling and sarcomeric proteins in response to beta-adrenergic stimulation leading to increased myocardial contractility and performance. The catalytic activity of PKA is tightly regulated by regulatory subunits that inhibit the catalytic subunit until released by cAMP binding. Phosphorylation of type II regulatory subunits promotes PKA activation; however, the role of phosphorylation in type I regulatory subunits remain uncertain. Here, we utilize human induced pluripotent stem cell cardiomyocytes (iPSC-CMs) to identify STK25 as a kinase of the type Iα regulatory subunit PRKAR1A. Phosphorylation of PRKAR1A leads to inhibition of PKA kinase activity and increased binding to the catalytic subunit in the presence of cAMP. *Stk25* knockout in mice diminishes Prkar1a phosphorylation, increases Pka activity, and augments contractile response to beta-adrenergic stimulation. Together, these data support STK25 as a negative regulator of PKA signaling through phosphorylation of PRKAR1A.

In brief

*Correspondence: bmf2002@cumc.columbia.edu.

AUTHOR CONTRIBUTIONS

X.Z., B.Z.W. and B.F. conceived and designed research; X.Z., B.Z.W., M.K., T. R.N., B.L., and J.R. performed experiments; R.K.S. performed mass spectrometry proteomics and analysis; J.R. was responsible for animal maintenance; R.L., M.T., J.B., and E.L. performed data analysis; X.Z. and B.Z.W. prepared figures; X.Z. and B.F. drafted the manuscript; B.Z.W., M.K., T.R.N., B.L., J.R., R.L., M.T., R.K.S., J.B., E.L., and G.V.-N. edited and revised manuscript; B.F. approved the final version of manuscript.

SUPPLEMENTAL INFORMATION

Supplemental information can be found online at https://doi.org/10.1016/j.celrep.2022.111203.

DECLARATION OF INTERESTS

The authors declare no competing interests.

INCLUSION AND DIVERSITY

We worked to ensure sex balance in the selection of non-human subjects. One or more of the authors of this paper self identifies as an underrepresented ethnic minority in science. One or more of the authors of this paper self identifies as a member of the LGBTQ+ community.

Zhang et al. use both *in vitro* and *in vivo* cardiomyocyte models to demonstrate that STK25 phosphorylates the type Iα regulatory subunit of PKA, PRKAR1A. This leads to increased inhibition of PKA signaling and attenuation of cAMP-mediated increases in cardiac contractile function.

Graphical Abstract

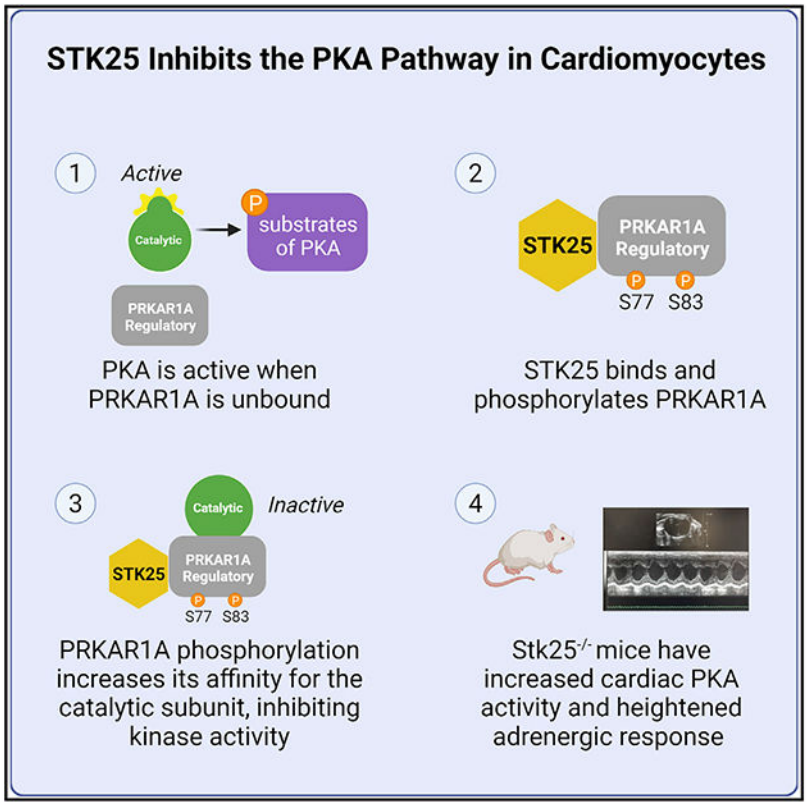

INTRODUCTION

Second messengers are key relays in the transduction of external cues into intracellular signaling cascades. cAMP is a prototypical second messenger generated downstream from G-protein-coupled receptors and is involved in integrating a diverse set of signaling pathways (Gancedo, 2013). The classic and most widely studied effector of cAMP is protein kinase A (PKA), and it has been broadly implicated in a diverse set of cellular processes including the cell cycle, proliferation, cytoskeletal dynamics, ion flux, and beta-adrenergic signaling (Tasken and Aandahl, 2004; Taylor et al., 2012). Specificity of signaling in a system with such a broad set of substrates relies on careful regulation of both cAMP metabolism as well as compartmentalization of PKA through a series of A-kinase anchoring proteins (AKAPs) (Colledge and Scott, 1999). These AKAPs bind to the regulatory subunits of PKA and direct its activity to a discrete set of effectors and substrates, thereby allowing for enhanced spatiotemporal control over PKA and the pathways it activates.

The PKA holoenzyme is comprised of a regulatory subunit dimer and two catalytic units (Kim et al., 2007). The main function of the regulatory subunit is to inactivate kinase activity in the absence of cAMP. There are two classes of regulatory subunits, type I and type II, each with an alpha and beta isoform. Binding of cAMP to the C-terminal tandem cAMP-binding domains of the regulatory subunits releases the catalytic domain, allowing for kinase activity (Barradeau et al., 2002). Type II regulatory subunits have a PKA substrate motif in the N terminus (RRXS), which is phosphorylated by the catalytic subunit upon binding to cAMP, enhancing its release and activation (Taylor et al., 1990). They also are the primary target of AKAPs, binding at nanomolar affinities (Colledge and Scott, 1999). The regulation of type I subunits, however, remains less well understood. They contain a pseudo-substrate (RRXxA/G) sequence that cannot be phosphorylated by the catalytic subunit. Although phosphorylation of the type I subunits has been reported as part of large phosphoproteomic projects, their role in regulation of PKA activity has not been demonstrated *in vivo* (Daub et al., 2008; Olsen et al., 2006, 2010; Oppermann et al., 2009; Zhou et al., 2013). Furthermore, the vast majority AKAP proteins do not interact with type I subunits, and the dual specificity AKAP proteins that do interact with type I subunits do so with significantly lower affinities compared with type II subunits.

In the heart, PKA mediates beta-adrenergic activation of the physiologic flight or fight response, modulating both heart rate and myocardial contractility (Wang et al., 2018). Substrates of PKA in the cardiomyocyte include troponin (TNNT2), myosin-binding protein c (MYBPC3), phospholamban (PLN), and ryanodine receptor (RYR2) (Marks, 2013). Acute activation of PKA in hyperadrenergic states leads to improved calcium flux and myocardial performance and is necessary for increases in stroke volume to meet cardiac output demands. In heart failure, chronic beta-adrenergic stimulation from high levels of catecholamines results in compensatory downregulation of beta-adrenergic signaling, leading to diminished phosphorylation of several PKA substrates (Bristow et al., 1982; Piacentino et al., 2003). Long-term activation of Pka was shown to be deleterious in mouse models and is thought to underly the maladaptive remodeling of chronic beta-adrenergic activation in heart failure (Antos et al., 2001).

STK25 is a stress response kinase in the sterile-20 (Ste20) kinase superfamily and has been shown through a series of *in vivo* models to impact glucose utilization, insulin homeostasis, and lipid metabolism (Amrutkar et al., 2015a, 2015b, 2016a, 2016b; Cansby et al., 2013; Chursa et al., 2017; Nerstedt et al., 2012; Nunez-Duran et al., 2017; Sutt et al., 2018). Overexpression of STK25 leads to steatosis and was shown to aggravate atherosclerosis in a PCSK9 gain-of-function mouse model (Cansby et al., 2018). Recently, STK25 was shown to interact with the Hippo signaling via phosphorylation of LATS1/2 and/or regulation of SAV1-STRIPAK (Bae et al., 2020; Lim et al., 2019). In this study, we use a combination of *in vitro* and *in vivo* cardiomyocyte models to demonstrate that STK25 phosphorylates the type Iα regulatory subunit of PKA, PRKAR1A. This leads to increased inhibition of PKA signaling, revealing a new regulatory mechanism that can control PKA activity and attenuate cAMP-mediated increases in cardiac contractile function.

RESULTS

STK25 inhibits PKA signaling

As part of a kinome knockout discovery project, CRISPR-Cas9 was used to generate a homozygous knockout of *STK25* in the wild-type induced pluripotent stem cell (iPSC) line WTC11 (Bruce Conklin, Gladstone Institute) (Hayashi et al., 2016), and cardiomyocytes were differentiated and characterized using an established protocol (Burridge et al., 2014). *STK25* expression in iPSC-derived cardiomyocytes was found to be similar to *Stk25* expression to primary cardiomyocytes from adult mice (Figures S1A and S1B). To identify potential substrates of STK25 in cardiomyocytes, mass-spectrometry-based phosphoproteomics was performed with $STK25^{+/+}$ and $STK25^{-/-}$ cardiomyocytes (Figure 1A). Signaling pathways impacted by *STK25* were identified using Ingenuity Pathway Analysis (Qiagen). A decrease in Hippo signaling was observed in response to loss of STK25, confirming a prior study demonstrating that STK25 activates the Hippo pathway (Figure 1B) (Lim et al., 2019). The most significant signaling change in response to loss of *STK25* was an upregulation of the PKA pathway. Several downstream substrates of PKA displayed increased phosphorylation including MYBPC3, TNNT2, RYR2, CACNA1C, and GSK3α (Table 1). $STK25^{-/-}$ cardiomyocytes exhibited increased PKA kinase activity when stimulated with the adenylate cyclase agonist forskolin (Figure 1C). In heterologous overexpression studies in HEK293T cells, STK25 decreased forskolin-induced PKA activity. This inhibition was dependent on the kinase domain of STK25, as overexpression of the kinase-dead mutant $STK25^{K49R/T174A}$ (Preisinger et al., 2004) did not inhibit PKA activity in response to forskolin (Figure 1D).

STK25 phosphorylates PRKAR1A

Two of the most downregulated phosphorylation sites in $STK25^{-/-}$ iPSC cardiomyocytes (iPSC-CMs) were S77 and S83 of PRKAR1A, raising the possibility that these sites were directly phosphorylated by STK25 (Table 1). PRKAR1A is the R1α member of the regulatory subunit isoforms of the PKA holoenzyme, which binds to and inhibits the catalytic subunit of PKA (PRKACA) and has been shown to disengage in response to cAMP, leading to PKA activation (Bossis and Stratakis, 2004). We first confirmed the phosphoproteomic data by demonstrating decreased phosphorylation of S77 and S83 in $STK25^{-/-}$ cardiomyocytes by immunoblot protein analysis (Figures 2A and S1C). In order to determine if this observation was dependent on the kinase activity of STK25, $STK25^{K49R/T174A}$ was expressed in $STK25^{-/-}$ iPSC-CMs and led to significantly decreased phosphorylation of S77 and S83 compared with overexpression of wild-type STK25 (Figures 2B and S1D). Stimulation of PKA with forskolin led to diminished phosphorylation at both S77 and S83 in $STK25^{+/+}$ iPSC-CMs but did not have a significant effect on $STK25^{-/-}$ iPSC-CMs (Figures 2C and S1E).

Co-immunoprecipitation experiments demonstrated STK25 and PRKAR1A binding using an epitope-tagged protein in HEK293T cells (Figure 2D). Though forskolin inhibited binding between PRKAR1A and the catalytic subunit PRKACA, it did not alter the association between STK25 and PRKAR1A (Figure 2E). Mutation of the kinase domain of STK25 also did not affect binding to PRKAR1A by immunoprecipitation (Figure S1F).

Using purified protein in an *in vitro* kinase assay, STK25 was able to phosphorylate PRKAR1A at S77 and S83 (Figure 2F).

Phosphorylation of S77/S83 inhibits PKA activity

Phosphorylation at S77 and S83 on PRKAR1A have been described as part of large-scale global phosphoproteomic experiments (Bian et al., 2014; Daub et al., 2008; Olsen et al., 2006; Oppermann et al., 2009), but their influence on PKA activity has not been characterized. In order to investigate the effect of pS77 and pS83 on the ability of PRKAR1A to inhibit PKA activity, phosphomimetic (S77E/S83E) and non-phosphomimetic (S77A/S83A) mutations were generated in PRKAR1A expression vectors. In HEK293T co-immunoprecipitation experiments, all three isoforms bind PRKACA similarly (Figures S2A and S2B). However, upon stimulation with forskolin, the S77E/S83E mutant exhibited elevated binding to the catalytic subunit compared with the S77A/S83A and wild-type (WT) PRKAR1A, indicating that positive charges at this residue may interfere with release of PKA in response to cAMP (Figures 3A and S2C). We then further tested this hypothesis by assessing PKA kinase activity *in vitro* in response to overexpression of these constructs in HEK293T cells. Though both WT and S77A/S83A PRKAR1A exhibited attenuated increases in induced PKA activity, expression of the S77E/S83E mutant exhibited no increase in PKA activity in response to forskolin (Figure 3B). Similarly, S77E/S83E PRKAR1A was able to inhibit metabolic activity of HEK293T in response to forskolin (Figure 3C) and in normal growth conditions (Figure S2D) to a significantly greater degree than either PRKAR1A or STK25 overexpression alone. In order to confirm that PRKAR1A is downstream of STK25, STK25 was overexpressed simultaneously with knockdown of PRKAR1A, resulting in rescue of STK25 inhibition of PKA activity (Figures 3Dand S2E). Together these data demonstrate a new regulatory event where STK25 phosphorylation increases the ability of PRKAR1A to bind the catalytic subunit and inhibit PKA activity in response to cAMP (Figure 3E).

Phosphorylation of PRKAR2A was also detected in our phosphoproteomic analysis; however, its phosphorylation levels increased with the loss of STK25 (Table 1). Despite this, given its role in PKA regulation in cardiomyocytes, we evaluated PKA holoenzyme activity from PRKAR1A and PRKAR2A immunoprecipitates. Loss of STK25 increased PKA activity from PRKAR1A complexes but not from PRKAR2A complexes (Figures S2F and S2G). Furthermore, immunoprecipitation experiments did not demonstrate binding of PRKAR2A and STK25 (Figure 2D). Together, these data do not support PRKAR2A as a downstream effector of STK25.

Stk25 loss increases PKA activity *in vivo*

In order to validate the STK25-PKA relationship *in vivo*, we generated a *Stk25*$^{-/-}$ mouse and investigated the impact of *Stk25* loss on the Pka pathway *in vivo*. Protein analysis demonstrated that loss of *Stk25* was accompanied by an increase in Prkar1a levels and a significant decrease in the ratio of pS77 and pS83 to total Prkar1a (Figures 4A and S3A). Whole-heart lysates of *Stk25*$^{-/-}$ mice displayed increased levels of Pka kinase activity compared with WT littermates (Figure 4B). Hearts histologically were similar without any

fibrosis (Figure S3B), and the heart weight to body weight ratios were not different between genotypes (Figure S3C).

Since Pka mediates beta-adrenergic stimulation of cardiomyocyte contraction function *in vivo*, we assessed the impact of *Stk25* loss on cardiac function in response to the β1 agonist isoproterenol using echocardiography. At baseline, there were no significant differences in either contractile function or chamber dimensions between genotypes; however, *Stk25*$^{-/-}$ mice displayed statistically greater individual increases in ejection fraction (EF) and fractional shortening (FS) and trends toward decreased chamber size in response to isoproterenol (Figures 4C, 4D, and S3D). Phosphorylation levels of downstream Pka effectors were also evaluated in response to isoproterenol, and loss of Stk25 was associated with significant increases in isoproterenol induced phosphorylation of Pln, TnI, and Ryr2, while CamkII remained unchanged (Figures S4A and S4B).

Because prolonged Pka activation has been associated with heart failure (Antos et al., 2001; Kushnir et al., 2010), a survival cohort of mice at 52 weeks were evaluated by echocardiography, and no significant differences in either heart function or left ventricular size were found (Figure S4C). We then investigated human heart failure samples and found that *STK25* expression was broadly increased in myocardial samples from patients with end-stage heart failure when compared with normal heart samples (Figure 4E; Table S1). Using available protein samples from this heart failure cohort, we analyzed the phosphorylation status of PRKAR1A and observed a concordant increase in STK25, PRKAR1A, and phosphorylated PRKAR1A. This raises the possibility that upregulation of STK25 and PRKAR1A has a role in heart failure and may be involved in the compensatory downregulation of beta-adrenergic signaling.

DISCUSSION

Kinases are integral components of signal-transduction pathways, playing key roles in most cellular processes that are initiated by external cues. Therapeutic modulation of kinases has demonstrated success in many branches of medicine, highlighted especially by those that leverage inhibition of kinase cascades implicated in oncogenic processes. Within cardiovascular biology, kinases regulate ion handling, contractility, and metabolism, and their dysregulation is involved in many cardiovascular diseases (Clerk et al., 2007; Heineke and Molkentin, 2006; Vlahos et al., 2003). Several kinases including PKA, Ca^{2+} calmodulin-dependent kinase, protein kinase C, and PIP3 kinase have all been implicated in both physiologic and pathologic signaling (Dhalla and Muller, 2010). Despite this progress, kinase-directed therapy has not been developed successfully for cardiovascular diseases, and identifying new regulators of kinase pathways is an area of unrealized therapeutic potential.

Here, we present evidence that STK25 is an inhibitor of the PKA pathway, whose phosphorylation of a regulatory subunit drives inhibition of the catalytic subunit's kinase activity. Though phosphorylation of the type II regulatory subunits has been described in detail, little is known about phosphorylation of type I regulatory subunits. Phosphorylation at S103 *in vitro* has been shown to be mediated by protein kinase G and interferes potentially with binding to PRKACA (Haushalter et al., 2018). Phosphorylation at S83 has

been shown to modulate PRKAR1A's association with the replication factor c complex *in vitro*, the consequence of which is unknown (Gupte et al., 2006). In the model we propose, phosphorylation at S77 and S83 increases affinity of PRKAR1A for the catalytic subunit and inhibits cAMP-mediated PKA activity. This stands in contrast to the regulation of type II subunits whose phosphorylation promotes release of the catalytic subunit and thus enhances PKA activity.

Though chronic PKA activation has been associated with progression of heart failure in animal models (Marks, 2013), knockout of *Stk25* resulted in an increase in PKA activity without evidence of heart failure. This discrepancy merits discussion. First, it should be noted that heart failure mouse models overexpressing the catalytic PKA subunit generate up to 8-fold increases in PKA activity, while in our model, mice experience approximately a 1.6-fold increase in PKA activity. This is in range of prior work demonstrating no heart failure phenotype with *Prkar1a* heterozygosity despite an increase in PKA activity by approximately 1.4-fold (Liu et al., 2020). Furthermore, data from human heart failure samples demonstrate decreased phosphorylation of PKA targets (Najafi et al., 2016), as chronic hyperstimulation of the beta-adrenergic receptor leads to desensitization and what is thought to be decreased PKA substrate activation (Ungerer et al., 1993). We observe increased levels of STK25 and phosphorylated PRKAR1A in heart failure samples. This would translate into suppression of PKA stimulation, yet it remains to be seen whether these changes are protective (e.g., as part of a downregulation response to hyperadrenergic state of heart failure) versus maladaptive (e.g., higher levels of STK25 lead to worsening cardiac performance) or both. While differences in either heart function or mortality are not observed with loss of *Stk25*, further longitudinal studies with overlayed chronic heart failure models are needed to determine if sustained STK25 loss is a potential therapeutic to improve cardiac function safely.

Limitations of the study

There are several important limitations to this study. How exactly phosphorylation of PRKAR1A alters its ability to inhibit the catalytic subunits remains unclear. We observe increased binding of S77E/S83E to the catalytic subunits in forskolin-stimulated cells, which implies there is either increased affinity between PRKAR1A and the catalytic subunit or decreased affinity for cAMP by phosphorylated PRKAR1A. Another possibility is a change in PRKAR1A's affinity for an AKAP. Though type I regulatory subunits generally have weak affinities for AKAP proteins and display a diffuse cytoplasmic localization, the impact that phosphorylation on the assembly of a larger macromolecular regulatory complex remains to be investigated. This is particularly relevant since forskolin did not inhibit PRKAR1A and STK25 binding, yet PRKAR1A phosphorylation was diminished. This would imply that there is either inhibition of STK25 kinase activity by cAMP or a phosphatase that acts on PRKAR1A that is stimulated by cAMP. Given that we observe residual phosphorylation of S77 and S83 in both iPSC-CM and mouse knockout studies, it is likely that there are other kinases that phosphorylate these sites and regulate PKA activity. Further studies are needed to identify kinases and phosphatases that modulate the phosphorylation of PRKAR1A and elucidate their physiological role in regulating PKA activity in the heart.

In summary, loss of *STK25* leads to increased PKA activity *in vitro* and *in vivo*. We identify PRKAR1A as a new substrate for STK25 and demonstrate that phosphorylation of PRKAR1A at S77 and S83 inhibits PKA signaling. Loss of Stk25 leads to increased physiologic response to beta-adrenergic stimulation of cardiac function without evidence of heart failure. Both STK25 and the phosphorylation of PRKAR1A are upregulated in heart failure and potentially represent a new pathway for downregulation of beta-adrenergic signaling in the heart.

STAR★METHODS

RESOURCE AVAILABILITY

Lead contact—Barry Fine, bmf2002@cumc.columbia.edu.

Materials availability—All unique reagents generated in this study are available from the lead contact with a completed materials transfer agreement.

Data and code availability

- RNA-seq data has been deposited in the Gene Expression Omnibus, NCBI: GSE195514 and proteomics data has been deposited in the PRIDE ProteomeXchange: PXD031367
- This paper does not report original code.
- Original data can be found at: https://data.mendeley.com/datasets/t2z9bkm78h/draft?a=a7e3489f-7112-4504-94a4-33f48aa43867
- Any additional information required to reanalyze the data reported in this paper is available from the lead contact upon request.

EXPERIMENTAL MODEL AND SUBJECT DETAILS

Cell culture—HEK293T cells (ATCC Cat# CRL-3216, RRID:CVCL_0063) were cultured in high glucose (4.5 g/L) DMEM supplemented with 10% FBS, penicillin and streptomycin, and grown in a CO_2 incubator maintained at atmospheric oxygen levels and 5% CO_2. Human induced pluripotent stem cells (hiPSC) were obtained through Material Transfer Agreements from Bruce Conklin, Gladstone Institute (WTC cell line). hiPSCs were expanded on growth factor reduced Matrigel-coated plates (Corning) in mTeSR plus medium (Stemcell technologies) containing mTeSR plus supplement (Stemcell technologies), 50U penicillin and 50U streptomycin. The cell culture medium was changed every other day, and cell passaged upon reaching 70% confluence. During the first 24 hrs after passaging, 5 μM Y-27632 dihydrochloride (Tocris, 1254) was supplemented to culture medium.

Animal studies—*Stk25* knockout mice were generated by CRISPR/Cas9 mediated genome engineering in C57BL/6J background (Jackson Laboratory, Bar Harbor, Maine). Exon 3–5 of Stk25 gene were deleted with two CRISPR guides from Synthego (sgRNA-stk25-7367 and sgRNA-stk25-10150). Both guides were mixed with IDT Cas9V3 protein to form RNP, which was further injected into the pronuclei of fertilized C57BL/6J eggs

to generate knockout founders. Genotyping was performed to show the *Stk25* knockout allele. Further breeding generated homozygous *Stk25*$^{-/-}$ mice and protein immunoblotting was performed to confirm an absence of Stk25. The protocol for all mouse experiments (AABC1503) was approved by the Columbia University Institutional Animal Care and Use Committee.

Cardiac function of 20 week and 52 week old mice was assessed by echocardiography by the Columbia University Mouse Imaging Core Facility (imaged by Visulasonics VEVO 3100 High Frequency Ultrasound imaging system and analyzed by Vevo LAB software). For 20 week old mice, cardiac function was recorded at baseline and 3 minutes after administration of the β-adrenergic receptor agonist isoproterenol (0.2ug/g, i.p.). Systolic function parameters including ejection fraction (EF, %), fractional shortening (FS, %), left ventricular end systolic diameter (LVESD, mm) and left ventricular end diastolic diameter (LVEDD, mm) were measured in the two-dimensional parasternal short-axis imaging plane of M-mode tracings close to the papillary muscle level. All animal experiments reported were conducted using 50% female and 50% male mice; littermates were used to reduce variation among batches of animals.

Patient samples—Patients with advanced HF were recruited at Columbia University Medical Center and heart tissue at the time of heart transplant was collected from the left ventricle. Control myocardial samples were obtained from the National Disease Research Interchange (https://ndriresource.org/ats) and were comprised of de-identified specimens collected from non-failing hearts determined to be unusable for cardiac transplantation due to non-cardiac donor issues but without evidence or knowledge of underlying cardiac disease. The study was approved by the Institutional Review Board of Columbia University (IRB# AAAR0055). All patients provided written informed consent before inclusion into the study.

METHOD DETAILS

CRISPR-Cas9—CRISPR-Cas9 Genome editing was used to generate a homozygous knockout of *STK25* in WTC iPSCs following the manufacturer's protocol (ORIGENE) with gRNA vector (KN203215G). Single-cell clones were expanded and confirmation of homozygous editing was determined by sanger sequencing of gDNA and protein analysis by western blot.

iPS cardiomyocyte differentiation—Cardiac differentiation of iPSC's was initiated in confluent monolayers two days after replating at a density of 200,000/cm^2 (24hrs in mTeSR plus medium with 5 μM Y-27632 dihydrochloride, followed by 24hrs in mTeSR plus medium without Y-27632). On day 0 of differentiation, media was changed to cardiac differentiation medium (CDM, consisting of RPMI-1640, Life Technologies), 500 μg/ml human recombinant albumin (Sigma), 213 μg/ml L-ascorbic acid (Sigma), 50U penicillin and 50U streptomycin) with 3–6 μM CHIR (4423, Tocris). 2 days after initial CHIR addition, media was changed to CDM with 2 μM Wnt-C59 (5148, Tocris). From day 4 onwards, media was changed fresh CDM every other day until cells start contracting. Media was then switched to RPMI-B27 (consisting of RPMI-1640, 1× B27 supplement

(Life Technologies), 213 μg/mL L-ascorbic acid, 50U penicillin and 50U streptomycin). Cardiomyocytes were characterized by flow cytometry using the cardiomyocyte-specific marker TNNT2 (BD Biosciences Cat# 565744, RRID:AB_2739341). Differentiation typically resulted in cell populations containing 80–90% TNNT2-positive cells at day 12.

PKA activity assay—PKA activity assay was performed using whole cell lysate from iPSC-CMs treated with either PBS or 10μM forskolin (Sigma-Aldrich, F6886) for 30 min at 37°C prior to assay, or immunoprecipitated type I and II PKA holoenzymes from iPSC-CMs whole cell lysate or whole heart lysates from *Stk25*$^{+/+}$ or *Stk25*$^{-/-}$ mice following the manufacturer's protocol (EIAPKA, Invitrogen). Briefly, PKA standards or diluted samples and reconstituted ATP were added into wells of PKA substrate plate. Phospho-PKA substrate antibody and Goat anti-Rabbit IgG HRP conjugate antibody were added into the wells per manufacturer protocol. After incubation TMB substrate was added into each well, and the plate was incubated for 30 min at room temperature. Stop solution was added, and absorbance at 450 nm was analyzed in a 96-plate reader.

Global phosphoproteomics analysis—Sorted *STK25*$^{+/+}$ and *STK25*$^{-/-}$ iPSC-CMs were lysed/homogenized by bead-beating in 8 M urea, 1%SDS and 200 mM EPPS (pH 8.5), protease, and phosphatase inhibitors. Lysates were cleared by centrifugation at 21,000 g for 30 min at 4°C, and protein concentration was measured by BCA. Proteins were reduced with 5 mM TCEP, alkylated with 10 mM iodoacetamide (IAA), and quenched with 10 mM DTT. A total of 500 μg of protein was chloroform–methanol precipitated. Protein was reconstituted in 200 mM EPPS (pH 8.5) and digested by Lys-C overnight and trypsin for 6 h, both at a 1:50 protease-to-peptide ratio. Digested peptides were quantified using a Nanodrop at 280 nm, and 200 μg of peptide from each sample were labeled with 800 μg TMT reagent using a 10-plex TMT kit (Navarrete-Perea et al., 2018). TMT labels were checked, 100 ng of each sample was pooled and desalted and analyzed by short SPS-MS3 method, and using normalization factor samples were bulk mixed at 1:1 across all channels and desalted using a 200 mg Sep-Pak solid-phase extraction column and dried using vacuum centrifugation.

Desalted isobaric labeled peptides were enriched for phospho-peptides using a mixture of MagReSyn Ti-IMAC and Zr-IMAC resins according ReSyn Bioscience instructions. In brief, 1.4 mg of labeled peptide were resuspended in 1 mL of binding buffer (80% Acetonitrile, 1M glycolic acid and 5% TFA) and incubated with equilibrated 150 μL (75 μL of each Ti-IMAC and Zr-IMAC) resins at room temperature for 30 min, and the resin was washed 3 three times to remove the unbound, non-phosphorylated peptides. Phospho-peptides were eluted using 1% ammonium hydroxide. The enriched phospho-peptides were further fractionated in eight fractions using Pierce High pH Reversed-Phase Peptide Fractionation Kit and each fraction dried down in a speed-vac.

The isobaric labeled dried phospho-peptides were resuspended in 10 μL of (3% acetonitrile/ 0.1% formic acid), and analyzed on an Orbitrap Fusion mass spectrometer coupled to a Dionex Ultimate 3000 (ThermoFisher Scientific) using the MSA-SPS-MS3 and NL SPS-MS3 method (Jiang et al., 2017). Peptides were separated on an EASY-Spray C18 50 cm column (Thermo Scientific). Peptide elution and separation were achieved at a non-linear flow rate of 250 nL/min using a gradient of 5–30% of buffer B (0.1% (v/v)

formic acid, 100% acetonitrile) for 110 min with a temperature of the column maintained at 50°C during the entire experiment. For both methods, MS1 data were collected using the Orbitrap (120,000 resolution; maximum injection time 50 ms; AGC 4×10^5). Determined charge states between 2 and 5 were required for sequencing and a 45 s dynamic exclusion window was used. Data-dependent top 10 MS2 scans were performed in the ion trap with collision-induced dissociation (CID) fragmentation (Turbo; NCE 35%; maximum injection time 60 ms; AGC 5×10^4). MS3 quantification scans were performed using the multi-notch MS3-based TMT method (ten SPS ions; 50,000 resolution; NCE 65% for MSA-SPS-TMT and 38% for NL-SPS-TMT maximum injection time 105 ms; AGC 1×10^5) using the Orbitrap.

Raw mass spectrometric data were analyzed using Proteome Discoverer 2.2 to perform database search and TMT reporter ions quantification. TMT tags on lysine residues and peptide N termini (+229.163 Da) and the carbamidomethylation of cysteine residues (+57.021 Da) was set as static modifications, while the oxidation of methionine residues (+15.995 Da), deamidation (+0.984) on asparagine and glutamine and phosphorylation (+79.966) on serine, threonine, and tyrosine were set as a variable modification. Data were searched against a UniProt Human database with peptide-spectrum match (PSMs) and protein-level FDR at 1% FDR. The signal-to-noise (S/N) measurements of each protein normalized so that the sum of the signal for all proteins in each channel was equivalent to account for equal protein loading. Phospho-peptides identification and quantification were imported into Perseus (Tyanova et al., 2016) for t test statistical analysis (FDR<0.05) to identify phospho-peptides demonstrating statistically significant changes in abundance. Pathway analysis were performed using Ingenuity Pathway Analysis (Qiagen).

iPS cardiomyocyte sorting—Cardiomyocytes were pretreated with 10μM of Y-27632 in B27 culture medium for 6 hrs, then digested with cell dissociation buffer (containing Hank's buffered saline solution, 100 Units/ml collagenase, 10μM Y-27632) at room temperature overnight. Cells were collected and centrifuged at 300 g for 5 min, and then resuspended in cell sorting buffer (CSB, containing Hank's buffered saline solution, 20 mM HEPES, 5% FBS, 10 units/ml Turbo DNase). The cell pellet was resuspended with anti-CD172a/b (SIRPα/β, 423107, Biolegend) and anti-CD90 (Thy-1, 11-0909-42, Invitrogen) antibodies in CSB to stain for 20 min at 4°C in the dark. Cells were washed 3 times with CSB and DAPI staining was added. Cardiomyocytes were sorted from the SIRPA+ and CD90-population and then plated on matrigel coated plates in B27 medium with 5μM Y-27632. The following day, medium was replaced with fresh B27, and cardiomyocytes generally started to beat in 2–5 days.

RNA isolation, sequencing, and analysis—RNA was extracted using the RNeasy Mini kit (Qiagen #74004) along with on-column DNAse digestion (Qiagen #79254). cDNA libraries were generated using the Clontech Ultra Low v4 kit followed by NextaraXT DNA Library Prep Kit, then sequenced on an Illumina NovaSeq 6000. Paired-end 100-bp sequenced reads were analyzed as follows: RTA (Illumina) software was used for base calling and bcl2fastq2 (version 2.19) for converting BCL to fastq format, coupled with adaptor trimming. A pseudoalignment to a kallisto index created from transcriptomes (build

GRCh38) using kallisto (0.44.0). After pseudoalignment the R package DESeq2 (1.28.1) was used to normalize the count matrix and calculate differentially expressed genes. Geneset enrichment analysis was performed using GSEA software (4.10.0) per documentation (Mootha et al., 2003; Subramanian et al., 2005).

siRNA and vector transfection—Cells were transfected using lipofectamine 3000 (Invitrogen) following the manufacturer's protocol with siRNA targeting STK25 (On-TargetPlus siRNA, Horizon Discovery, L-004873-00-0050) or siRNA targeting PRKAR1A (EHU071341, Sigma) for protein knockdown or non-targeting control siRNA (ON-TARGETplus non-targeting pool, Horizon Discovery D-001810-10-50) as scramble control.

For heterologous expression studies, cells were transfected using lipofectamine 3000 (Invitrogen, L3000015) following the manufacturer's protocol. Vectors used include Flag-WT-STK25 vector (EX-M0142-M46, GeneCopoeia), Flag-K49R/T147A-STK25 vector (Vector Builder), Flag-empty vector (EX-NEG-M46, GeneCopoeia), V5-PRKAR1A (Vector Builder, VB200124-1141aes), V5-S77A/S83A-PRKAR1A (Vector Builder, VB200124-1126jtp), and V5-S77E/S83E-PRKAR1A (Vector Builder, VB200124-1127pst).

qRT-PCR assays—Equivalent amounts (2 μg) of purified RNA were used as a template to synthesize cDNA using oligo-d(T) primers and SuperScript III First-Strand Synthesis SuperMix (Invitrogen, 18080400). *STK25* was quantified by real-time PCR using Fast SYBR Green mixture (Life Technologies, 4385612) and was carried out on Applied Biosystems Step One Plus. Relative levels were calculated using ΔΔCτ method. Data analysis was carried out using the fold change normalized to GAPDH gene expression.

Gene	Forward primer 5′-3′	Reverse primer 5′-3′
STK25	GCTCCTACCTAAAGAGCACCA	TGGCAATGTATGTCTCCTCCAG
GAPDH	GGACTCATGACCACAGTCCATG	CAGGGATGATGTTCTGGAGAGC

Immunoprecipitation and immunoblot analysis—300 μg of total protein from whole cell lysate were used in immunoprecipitation experiments. The extract was incubated with anti-Flag affinity gel (Sigma-Aldrich Cat# A2220, RRID:AB_10063035), anti-V5 affinity gel (Sigma-Aldrich Cat# A7345, RRID:AB_10062721), anti-PRKAR1A (Abcam Cat# ab139695, RRID:AB_2893184) or anti-PRKAR2A (ProteinTech Cat# 10142-2-AP) overnight at 4°C. The affinity gel beads were centrifuged at 8000xg for 1 min, washed three times in TBS buffer. The affinity gel beads were added with 4× Laemmli SDS sample buffer (NuPAGE), denatured at for 5 min at 95°C and analyzed by SDS-PAGE and immunoblotting. For Western blotting antibodies include: HRP conjugated anti-GAPDH (Cell Signaling Technology Cat# 3683, RRID:AB_1642205), anti-STK25 (Abcam Cat# ab157188, RRID:AB_2725788), anti-Flag (Sigma-Aldrich Cat# F3165, RRID:AB_259529), anti-GM130 (Cell Signaling Technology Cat# 12480, RRID:AB_2797933), anti-PRKAR1A (Abcam Cat# ab139695, RRID:AB_2893184), anti-pS77 PRKAR1A (Abcam Cat#ab139682, RRID:AB_2904566), anti-pS83 PRKAR1A (Abcam Cat#ab154851, RRID:AB_2904567), anti-PRKAR2A

(ProteinTech Cat# 10142-2-AP), anti-phospholamban (Cell Signaling Technology Cat# 14562, RRID:AB_2798511), anti-phospho-phospholamban -pS16/T17 (Cell Signaling Technology Cat# 8496, RRID:AB_10949102), anti-Ryanodine receptor 2 (Abcam Cat#ab196355, RRID:AB_2904568), anti-p-Ryanodine receptor 2-pS2808 (Abcam Cat# ab59225, RRID:AB_946327), anti-TnI (Cell Signaling Cat# 4002), anti-TnI-pS23/S24 (Cell Signaling Cat# 4004), anti-V5 (Sigma-Aldrich Cat# V8137, RRID:AB_261889), anti-PKA Catalytic subunit (Abcam Cat# ab26322, RRID:AB_2170049), HRP-conjugated anti-mouse (Cell Signaling Technology Cat# 7076, RRID:AB_330924) and HRP-conjugated anti-rabbit (Cell Signaling Technology Cat# 7074, RRID:AB_2099233) were used for detection.

***In vitro* kinase assay—**Recombinant protein STK25 (0.5μM, TP303215, OriGene) and PRKAR1A (1μM, TP303828 Origene) were mixed with *in vitro* kinase buffer (25 mM Tris-HCl, 10 mM beta-glycerophosphate, 10 mM $MgCl_2$, 20 mM NaF, 2 mM DTT, 1 mM sodium orthovanadate, 1 × Protease Inhibitor cocktail (Roche)) containing ATP (500uM) and incubated at 37°C for 30 min. *In vitro* kinase assay was terminated by adding Laemmli SDS sample buffer. Phosphorylation levels of PRKAR1A at S77 and S83 were analyzed by SDS-PAGE and immunoblotting.

Real Time Glo cell viability assay—Cells were seeded into 96-well plates at a density of 3000 cells per well 24 h before measurement. RealTime-Glo (Promega; G9712) reagent was added to each well per manufacturer protocol and measurement of luminescence was performed at selected time points on a BioTek Synergy JHTX with Gen5 data analysis software.

QUANTIFICATION AND STATISTICAL ANALYSIS

Statistical analyses were performed using Prism 8 (Graphpad Software). Results are presented as mean ± standard deviation. For comparisons between two groups, a two tailed unpaired t test was used unless otherwise specific. Welch's correction was utilized for two groups of unequal sizes. For multiple group comparisons, either one way or two-way (depending on the number of variables) ANOVA followed by multiple comparison post-hoc testing was performed as indicated using Prism 8. Notation in the text is as follows *$p < 0.05$, **$p < 0.01$, ***$p < 0.001$ and ****$p < 0.0001$.

Supplementary Material

Refer to Web version on PubMed Central for supplementary material.

ACKNOWLEDGMENTS

We would like to thank Qing Li for his surgical expertise, Erin Bush at the Columbia Genome Center for RNA sequencing (RNA-seq) help, Christopher Damoci at the Columbia Mouse Imaging Core Facility and the labs of Veli Top-kara, Elain Wan, and Emily Tsai for reagents, technical expertise, and tissue samples. B.F is supported by a grant from the NHLBI (K08HL140201), the Gerstner Foundation, and the Schwartz Foundation. G.V.-N. is supported by grants from the NIH (UH3EB025765, P41EB027062, and R01HL076485) and NSF (NSF16478). B.Z.W., T.R.N., and B.L. are supported by the MSTP Training Program (T32GM007367). B.L. is also supported by the NIH (F30HL145921). R.K.S. is supported by 2P30 CA013696-45 Cancer Center Support Grant. M.K. is supported by a Glorney Raisbeck Fellowship Award in Cardiovascular Disease.

REFERENCES

Amrutkar M, Cansby E, Chursa U, Nñnez-Durán E, Chanclón B, Ståhlman M, Fridén V, Mannerås-Holm L, Wickman A, Smith U, et al. (2015a). Genetic disruption of protein kinase STK25 ameliorates metabolic defects in a diet-induced type 2 diabetes model. Diabetes 64, 2791–2804. [PubMed: 25845663]

Amrutkar M, Cansby E, Nuñnez-Durán E, Pirazzi C, Ståhlman M, Stenfeldt E, Smith U, Borén J, and Mahlapuu M (2015b). Protein kinase STK25 regulates hepatic lipid partitioning and progression of liver steatosis and NASH. FASEB J. 29, 1564–1576. [PubMed: 25609431]

Amrutkar M, Chursa U, Kern M, Nuñez-Durán E, Ståhlman M, Sütt S, Borén J, Johansson BR, Marschall HU, Blüher M, and Mahlapuu M (2016a). STK25 is a critical determinant in nonalcoholic steatohepatitis. FASEB J. 30, 3628–3643. [PubMed: 27421788]

Amrutkar M, Kern M, Nuñez-Durán E, Ståhlman M, Cansby E, Chursa U, Stenfeldt E, Borén J, Blüher M, and Mahlapuu M (2016b). Protein kinase STK25 controls lipid partitioning in hepatocytes and correlates with liver fat content in humans. Diabetologia 59, 341–353. [PubMed: 26553096]

Antos CL, Frey N, Marx SO, Reiken S, Gaburjakova M, Richardson JA, Marks AR, and Olson EN (2001). Dilated cardiomyopathy and sudden death resulting from constitutive activation of protein kinase a. Circ. Res 89, 997–1004. [PubMed: 11717156]

Bae SJ, Ni L, and Luo X (2020). STK25 suppresses Hippo signaling by regulating SAV1-STRIPAK antagonism. Elife 9, e54863. [PubMed: 32292165]

Barradeau S, Imaizumi-Scherrer T, Weiss MC, and Faust DM (2002). Intracellular targeting of the type-I alpha regulatory subunit of cAMP-dependent protein kinase. Trends Cardiovasc. Med 12, 235–241. [PubMed: 12242045]

Bian Y, Song C, Cheng K, Dong M, Wang F, Huang J, Sun D, Wang L, Ye M, and Zou H (2014). An enzyme assisted RP-RPLC approach for indepth analysis of human liver phosphoproteome. J. Proteomics 96, 253–262. [PubMed: 24275569]

Bossis I, and Stratakis CA (2004). Minireview: PRKAR1A: normal and abnormal functions. Endocrinology 145, 5452–5458. [PubMed: 15331577]

Bray NL, Pimentel H, Melsted P, and Pachter L (2016). Near-optimal probabilistic RNA-seq quantification. Nat. Biotechnol 34, 525–527. [PubMed: 27043002]

Bristow MR, Ginsburg R, Minobe W, Cubicciotti RS, Sageman WS, Lurie K, Billingham ME, Harrison DC, and Stinson EB (1982). Decreased catecholamine sensitivity and beta-adrenergic-receptor density in failing human hearts. N. Engl. J. Med 307, 205–211. [PubMed: 6283349]

Burridge PW, Matsa E, Shukla P, Lin ZC, Churko JM, Ebert AD, Lan F, Diecke S, Huber B, Mordwinkin NM, et al. (2014). Chemically defined generation of human cardiomyocytes. Nat. Methods 11, 855–860. [PubMed: 24930130]

Cansby E, Amrutkar M, Mannerås Holm L, Nerstedt A, Reyahi A, Stenfeldt E, Borén J, Carlsson P, Smith U, Zierath JR, and Mahlapuu M (2013). Increased expression of STK25 leads to impaired glucose utilization and insulin sensitivity in mice challenged with a high-fat diet. FASEB J 27, 3660–3671. [PubMed: 23729594]

Cansby E, Magnusson E, Nuñez-Durán E, Amrutkar M, Pedrelli M, Parini P, Hoffmann J, Ståhlman M, Howell BW, Marschall HU, et al. (2018). STK25 regulates cardiovascular disease progression in a mouse model of hypercholesterolemia. Arterioscler. Thromb. Vasc. Biol 38, 1723–1737. [PubMed: 29930001]

Chursa U, Nuñez-Durán E, Cansby E, Amrutkar M, Sütt S, Ståhlman M, Olsson BM, Borén J, Johansson ME, Bäckhed F, et al. (2017). Overexpression of protein kinase STK25 in mice exacerbates ectopic lipid accumulation, mitochondrial dysfunction and insulin resistance in skeletal muscle. Diabetologia 60, 553–567. [PubMed: 27981357]

Clerk A, Cullingford TE, Fuller SJ, Giraldo A, Markou T, Pikkarainen S, and Sugden PH (2007). Signaling pathways mediating cardiac myocyte gene expression in physiological and stress responses. J. Cell. Physiol 212, 311–322. [PubMed: 17450511]

Colledge M, and Scott JD(1999). AKAPs: from structure to function.Trends Cell Biol. 9, 216–221. [PubMed: 10354567]

Daub H, Olsen JV, Bairlein M, Gnad F, Oppermann FS, Körner R, Greff Z, Kéri G, Stemmann O, and Mann M (2008). Kinase-selective enrichment enables quantitative phosphoproteomics of the kinome across the cell cycle. Mol. Cell 31, 438–448. [PubMed: 18691976]

Dhalla NS, and Müller AL (2010). Protein kinases as drug development targets for heart disease therapy. Pharmaceuticals 3, 2111–2145. [PubMed: 27713345]

Gancedo JM (2013). Biological roles of cAMP: variations on a theme in the different kingdoms of life. Biol. Rev. Camb. Philos. Soc 88, 645–668. [PubMed: 23356492]

Gupte RS, Traganos F, Darzynkiewicz Z, and Lee MYWT (2006). Phosphorylation of RIalpha by cyclin-dependent kinase CDK 2/cyclin E modulates the dissociation of the RIalpha-RFC40 complex. Cell Cycle 5, 653–660. [PubMed: 16582606]

Haushalter KJ, Casteel DE, Raffeiner A, Stefan E, Patel HH, and Taylor SS (2018). Phosphorylation of protein kinase A (PKA) regulatory subunit RIalpha by protein kinase G (PKG) primes PKA for catalytic activity in cells. J. Biol. Chem 293, 4411–4421. [PubMed: 29378851]

Hayashi Y, Hsiao EC, Sami S, Lancero M, Schlieve CR, Nguyen T, Yano K, Nagahashi A, Ikeya M, Matsumoto Y, et al. (2016). BMP-SMAD-ID promotes reprogramming to pluripotency by inhibiting p16/INK4A-dependent senescence. Proc. Natl. Acad. Sci. USA 113, 13057–13062. [PubMed: 27794120]

Heineke J, and Molkentin JD (2006). Regulation of cardiac hypertrophy by intracellular signalling pathways. Nat. Rev. Mol. Cell Biol 7, 589–600. [PubMed: 16936699]

Jiang X, Bomgarden R, Brown J, Drew DL, Robitaille AM, Viner R, and Huhmer AR (2017). Sensitive and accurate quantitation of phospho-peptides using TMT isobaric labeling technique. J. Proteome Res 16, 4244–4252. [PubMed: 29022350]

Kim C, Cheng CY, Saldanha SA, and Taylor SS (2007). PKA-I holoenzyme structure reveals a mechanism for cAMP-dependent activation. Cell 130, 1032–1043. [PubMed: 17889648]

Kushnir A, Betzenhauser MJ, and Marks AR (2010). Ryanodine receptor studies using genetically engineered mice. FEBS Lett. 584, 1956–1965. [PubMed: 20214899]

Lim S, Hermance N, Mudianto T, Mustaly HM, Mauricio IPM, Vittoria MA, Quinton RJ, Howell BW, Cornils H, Manning AL, and Ganem NJ (2019). Identification of the kinase STK25 as an upstream activator of LATS signaling. Nat. Commun. 10, 1547. [PubMed: 30948712]

Liu Y, Xia P, Chen J, Bandettini WP, Kirschner LS, Stratakis CA, and Cheng Z (2020). PRKAR1A deficiency impedes hypertrophy and reduces heart size. Physiol. Rep. 8, e14405. [PubMed: 32212257]

Love MI, Huber W, and Anders S (2014). Moderated estimation of fold change and dispersion for RNA-seq data with DESeq2. Genome Biol. 15, 550. [PubMed: 25516281]

Marks AR (2013). Calcium cycling proteins and heart failure: mechanisms and therapeutics. J. Clin. Invest. 123, 46–52. [PubMed: 23281409]

Mootha VK, Lindgren CM, Eriksson KF, Subramanian A, Sihag S, Lehar J, Puigserver P, Carlsson E, Ridderstråle M, Laurila E, et al. (2003). PGC-1alpha-responsive genes involved in oxidative phosphorylation are coordinately downregulated in human diabetes. Nat. Genet. 34, 267–273. [PubMed: 12808457]

Najafi A, Sequeira V, Kuster DWD, and van der Velden J (2016). beta-adrenergic receptor signalling and its functional consequences in the diseased heart. Eur. J. Clin. Invest. 46, 362–374. [PubMed: 26842371]

Navarrete-Perea J, Yu Q, Gygi SP, and Paulo JA (2018). Streamlined tandem mass tag (SL-TMT) protocol: an efficient strategy for quantitative (Phospho)proteome profiling using tandem mass tag-synchronous precursor selection-MS3. J. Proteome Res. 17, 2226–2236. [PubMed: 29734811]

Nerstedt A, Cansby E, Andersson CX, Laakso M, Stančáková A, Blüher M, Smith U, and Mahlapuu M (2012). Serine/threonine protein kinase 25 (STK25): a novel negative regulator of lipid and glucose metabolism in rodent and human skeletal muscle. Diabetologia 55, 1797–1807. [PubMed: 22391949]

Nuñez-Durán E, Chanclón B, Sütt S, Real J, Marschall HU, Wernstedt Asterholm I, Cansby E, and Mahlapuu M (2017). Protein kinase STK25 aggravates the severity of non-alcoholic fatty pancreas disease in mice. J. Endocrinol. 234, 15–27. [PubMed: 28442507]

Olsen JV, Blagoev B, Gnad F, Macek B, Kumar C, Mortensen P, and Mann M (2006). Global, in vivo, and site-specific phosphorylation dynamics in signaling networks. Cell 127, 635–648. [PubMed: 17081983]

Olsen JV, Vermeulen M, Santamaria A, Kumar C, Miller ML, Jensen LJ, Gnad F, Cox J, Jensen TS, Nigg EA, et al. (2010). Quantitative phosphoproteomics reveals widespread full phosphorylation site occupancy during mitosis. Sci. Signal. 3, ra3. [PubMed: 20068231]

Oppermann FS, Gnad F, Olsen JV, Hornberger R, Greff Z, Kéri G, Mann M, and Daub H (2009). Large-scale proteomics analysis of the human kinome. Mol. Cell. Proteomics 8, 1751–1764. [PubMed: 19369195]

Piacentino V 3rd, Weber CR, Chen X, Weisser-Thomas J, Margulies KB, Bers DM, and Houser SR (2003). Cellular basis of abnormal calcium transients of failing human ventricular myocytes. Circ. Res. 92, 651–658. [PubMed: 12600875]

Preisinger C, Short B, De Corte V, Bruyneel E, Haas A, Kopajtich R, Gettemans J, and Barr FA (2004). YSK1 is activated by the Golgi matrix protein GM130 and plays a role in cell migration through its substrate 14-3-3zeta. J. Cell Biol. 164, 1009–1020. [PubMed: 15037601]

Subramanian A, Tamayo P, Mootha VK, Mukherjee S, Ebert BL, Gillette MA, Paulovich A, Pomeroy SL, Golub TR, Lander ES, and Mesirov JP (2005). Gene set enrichment analysis: a knowledge-based approach for interpreting genome-wide expression profiles. Proc. Natl. Acad. Sci. USA 102, 15545–15550. [PubMed: 16199517]

Sütt S, Cansby E, Paul A, Amrutkar M, Nuñez-Durán E, Kulkarni NM, Ståhlman M, Borén J, Laurencikiene J, Howell BW, et al. (2018). STK25 regulates oxidative capacity and metabolic efficiency in adipose tissue. J. Endocrinol. 238, 187–202. [PubMed: 29794231]

Tasken K, and Aandahl EM (2004). Localized effects of cAMP mediated by distinct routes of protein kinase A. Physiol. Rev. 84, 137–167. [PubMed: 14715913]

Taylor SS, Buechler JA, and Yonemoto W (1990). cAMP-dependent protein kinase: framework for a diverse family of regulatory enzymes. Annu. Rev. Biochem. 59, 971–1005. [PubMed: 2165385]

Taylor SS, Ilouz R, Zhang P, and Kornev AP (2012). Assembly of allosteric macromolecular switches: lessons from PKA. Nat. Rev. Mol. Cell Biol. 13, 646–658. [PubMed: 22992589]

Tyanova S, Temu T, Sinitcyn P, Carlson A, Hein MY, Geiger T, Mann M, and Cox J (2016). The Perseus computational platform for comprehensive analysis of (prote)omics data. Nat. Methods 13, 731–740. [PubMed: 27348712]

Ungerer M, Böhm M, Elce JS, Erdmann E, and Lohse MJ (1993). Altered expression of beta-adrenergic receptor kinase and beta 1-adrenergic receptors in the failing human heart. Circulation 87, 454–463. [PubMed: 8381058]

Vlahos CJ, McDowell SA, and Clerk A (2003). Kinases as therapeutic targets for heart failure. Nat. Rev. Drug Discov. 2, 99–113. [PubMed: 12563301]

Wang J, Gareri C, and Rockman HA (2018). G-Protein-Coupled receptors in heart disease. Circ. Res. 123, 716–735. [PubMed: 30355236]

Zhou H, Di Palma S, Preisinger C, Peng M, Polat AN, Heck AJR, and Mohammed S (2013). Toward a comprehensive characterization of a human cancer cell phosphoproteome. J. Proteome Res. 12, 260–271. [PubMed: 23186163]

Highlights

- Loss of STK25 in iPSC-derived cardiomyocytes upregulates PKA signaling
- STK25 binds to and phosphorylates the PKA regulatory subunit PRKAR1A at S77 and S83
- Phosphorylation of PRKAR1A inhibits PKA activity through increased affinity for PRKACA
- Stk25 loss in mice increases PKA activity *in vivo* upon β-adrenergic stimulation

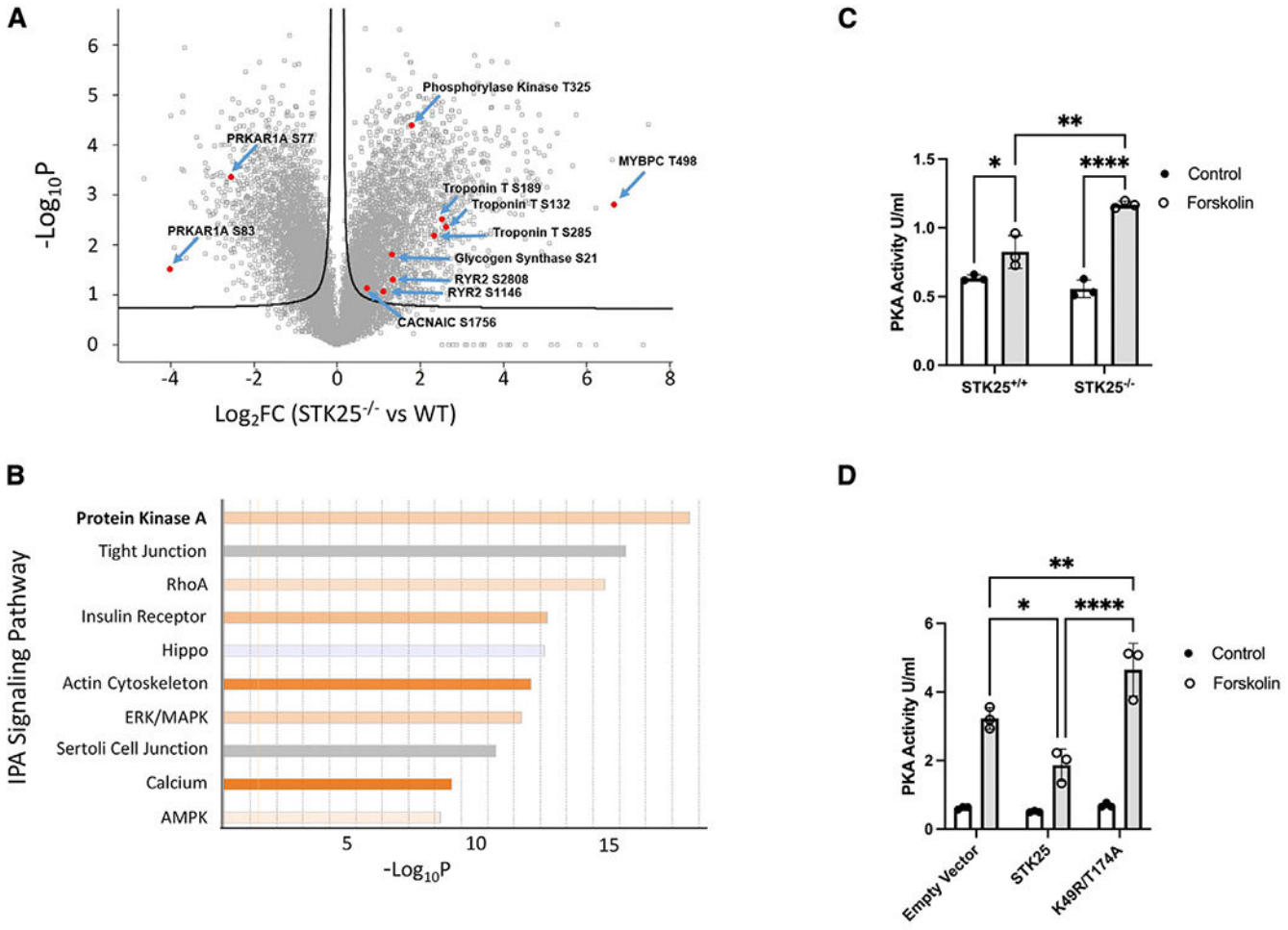

Figure 1. STK25 inhibits PKA activity

(A) Differential phosphoproteomic spectra of *STK25*$^{+/+}$ and *STK25*$^{-/-}$ cardiomyocytes. Members of the PKA signaling pathway are highlighted.

(B) Ingenuity phosphoprotein pathway analysis. Orange indicates pathways upregulated in *STK25*$^{-/-}$ cardiomyocytes, while blue indicates upregulation in *STK25*$^{+/+}$.

(C) PKA activity in response to 10 μM forskolin treatment for 30 min in *STK25*$^{+/+}$ and *STK25*$^{-/-}$ cardiomyocytes. n = 3 for each condition.

(D) PKA activity in response to 10 μM forskolin treatment for 30 min in HEK293T cells overexpressing either empty vector, wild-type STK2,5 or kinase-dead K49R/T174A. n = 3 for each.

Bar graph data are represented as mean ± SD and analyzed in technical triplicates, *p < 0.05, **p < 0.01, ****p < 0.0001 using ANOVA and Tukey's adjustment for multiple comparisons.

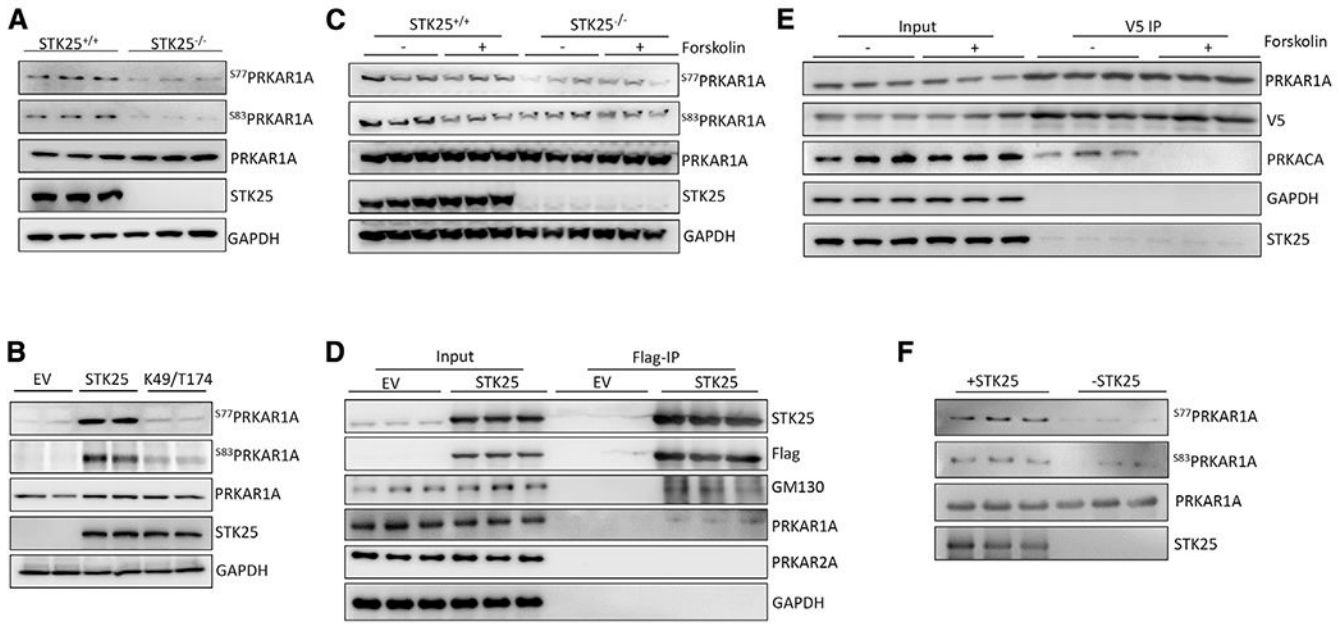

Figure 2. STK25 binds to and phosphorylates PRKAR1A

(A) Immunoblot of PRKAR1A phospho-S77 and -S83 in *STK25*$^{+/+}$ and *STK25*$^{-/-}$ cardiomyocyte protein lysates. n = 3 for each condition.

(B) Immunoblots of phosphor-S77 and -S83 of PRKAR1A in *STK25*$^{-/-}$ cardiomyocytes transfected with empty vector (EV), wild-type STK25, and kinase dead K49R/T174A STK25. n = 2 for each condition.

(C) Forskolin (10 μM, 30 min)-stimulated *STK25*$^{+/+}$ and *STK25*$^{-/-}$ cardiomyocytes immunoblotted for phosphorylation of PRKAR1A. n = 3 for each condition.

(D) Immunoprecipitation of FLAG-STK25 expressed in HEK293T cells and immunoblotted for PRKAR1A, PRKA2A, and GM130 (positive control binding partner). n = 3 for each condition.

(E) Co-immunoprecipitation of PRKAR1A-V5 with STK25 and PRKACA in HEK293T cells treated with forskolin (10 μM, 30 min). n = 3 for each condition.

(F) *In vitro* kinase assay of purified STK25 and PRKAR1A, immunoblotted for phosphorylation of S77 and S83 of PRKAR1A. n = 3 for each condition.

See also Figure S1.

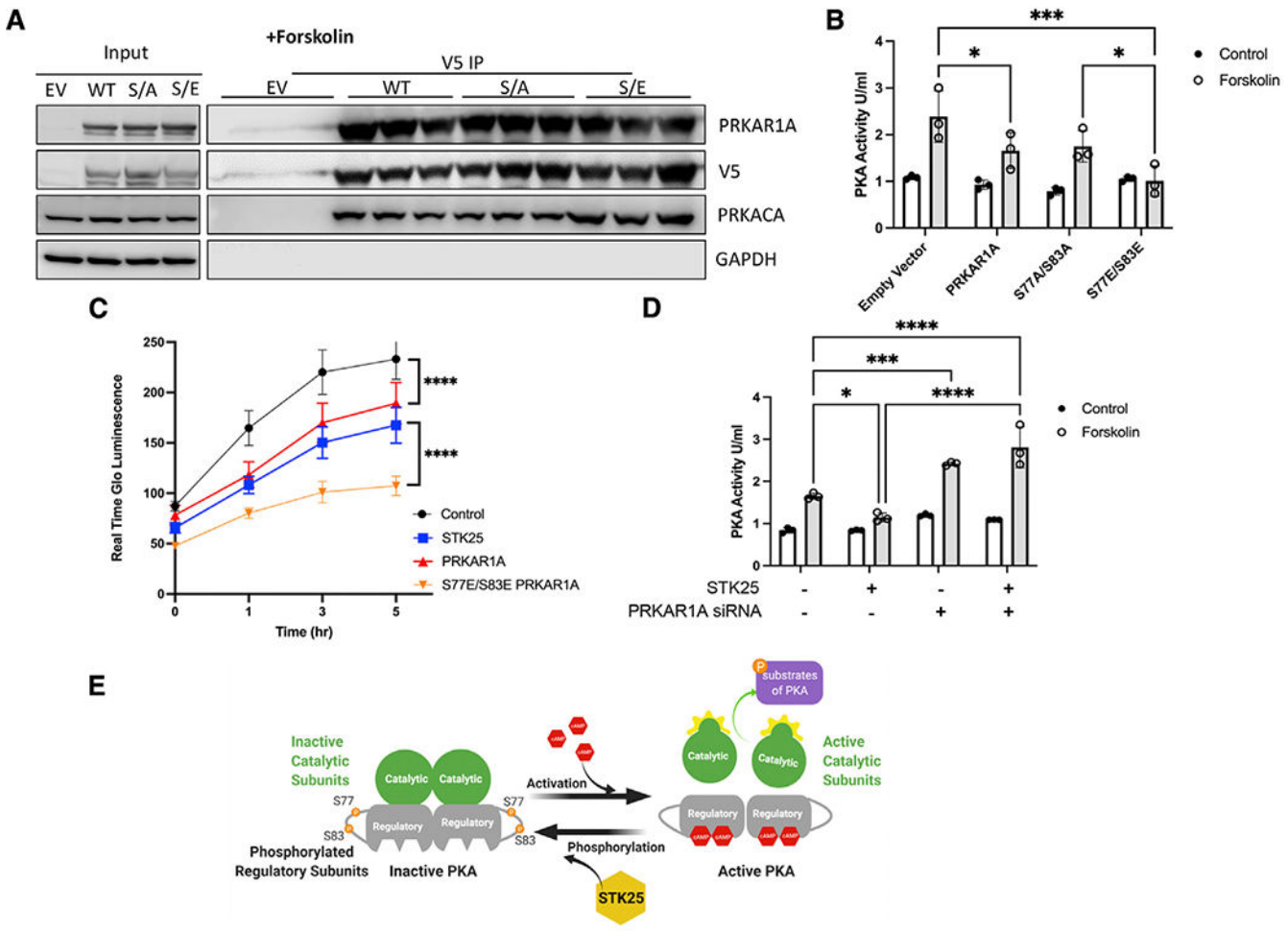

Figure 3. Phosphorylation of PRKAR1A inhibits PKA activity

(A) Co-immunoprecipitations of V5-tagged PRKAR1A, S77A/S83A PRKAR1A, or S77E/S83 PRKAR1A and immunoblotting for PRKARCA in HEK293T cells stimulated with forskolin (10 μM, 30 min). n = 3 for each condition.

(B) PKA activity in HEK293T cells stimulated with forskolin (10 μM, 30 min) and transfected with EV, wild-type PRKAR1A, S77A/S83A PRKAR1A mutant, or S77E/S83E PRKAR1A mutant as indicated.

(C) HEK293T cells transfected with the indicated vectors and assessed for growth by Real Time Glo for 5 h after stimulation with forskolin (10 mM). A representative Real Time Glo assay analyzed in sextuplicate ±SEM is shown.

(D) PKA activity in HEK293T cells stimulated with forskolin (10 μM, 30 min) and either overexpressing STK25 and/or the siRNA of PRKAR1A.

(E) Model of STK25 downregulation of the PKA pathway through phosphorylation of PRKAR1A.

For all graphs in this figure, n = 3 for each condition, data are presented as mean ± SD and analyzed in technical triplicates, *p < 0.05, ***p < 0.001, and ****p < 0.0001 by ANOVA with Tukey's adjustment for multiple comparisons.

See also Figure S2.

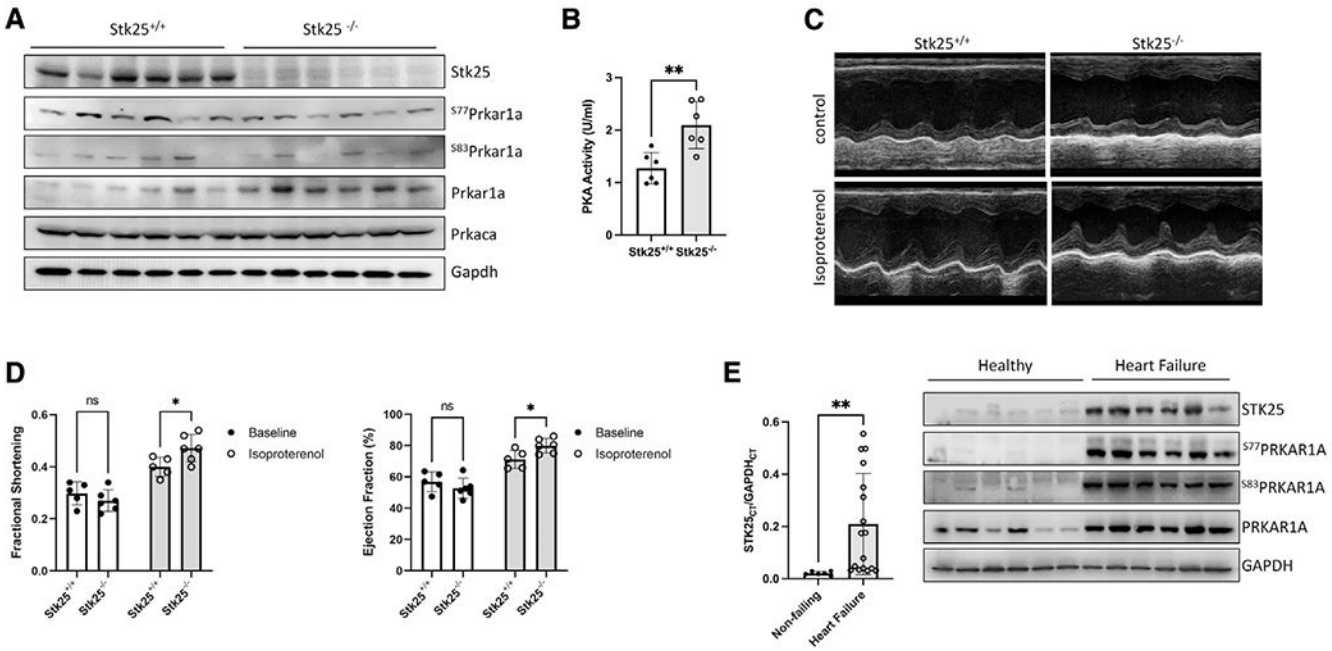

Figure 4. Stk25 loss increases response to adrenergic stimulation *in vivo*

(A) Immmunoblot of Stk25, Prkaca, Gapdh, phospho-S77, phospho-S83, and total Prkar1a in *Stk25*$^{+/+}$ and *Stk25*$^{-/-}$ whole-heart lysates.

(B) *Stk25*$^{+/+}$ and *Stk25*$^{-/-}$ mouse heart lysates were assessed for PKA activity *in vitro*.

(C) Representative m-mode images of *Stk25*$^{+/+}$ and *Stk25*$^{-/-}$ mouse hearts stimulated with either control or isoproterenol.

(D) Echocardiographic measurements of ejection fraction (EF) and fractional shortening (FS) at unstimulated baseline and in response to isoproterenol, n = 5 for *Stk25*$^{+/+}$ and n = 6 for *Stk25*$^{-/-}$.

(E) RT-PCR (left) from left ventricular myocardium of normal hearts (n = 6) or heart failure (n = 17) expressed as a ratio of the threshold cycle curve (Ct) of *STK25* to *GAPDH*. Immunoblot (right) of STK25 and PRKAR1A expression and phosphorylation in protein lysates from left ventricular myocardium of normal hearts or failing hearts.

Bar graphs presented as mean ± SD and analyzed in technical triplicates, *p < 0.05, **p < 0.01 by Student's t test in (B), repeated measures two-way ANOVA with Sidak's correction for multiple comparisons in (D), and Welch's t test in (E).

See also Figures S3 and S4 and Table S1.

Table 1.

PKA pathway phosphoproteomic changes in STK25$^{-/-}$ compared with wild type

Function		Protein descriptions		Fold change	Phosphorylation sites	Protein accessions
PKA	regulatory subunits	PRKAR1A	cAMP-dependent protein kinase type I alpharegulatory subunit	0.17	S77, S83	P10644
		PRKAR2A	cAMP-dependent protein kinase type II-alpha regulatory subunit	3.03	S78	P13861
	catalytic subunit	PRKACA	cAMP-dependent protein kinase catalytic subunit alpha	0.79	S339	P17612
PKA targets	contractility Ca^{2+} handling	MYBPC3	myosin-binding protein C, cardiac type	100.03	T498	Q14896
		TNNT2	troponin T, cardiac muscle	6.18	S132	P45379
				5.75	S285	
				5.02	S189	
		RYR2	isoform 2 of ryanodine receptor 2	2.51	S2808	Q92736
				2.14	S4368	
		CACNA1C	isoform 2 of voltage-dependent L-type calcium channel subunit alpha 1C	1.65	S1756	Q13936
	energy metabolism	PHKG2	phosphorylase b kinase gamma catalytic chain	3.48	T325	P15735
		GSK3α	glycogen synthase kinase-3 alpha	2.50	S21	P49840
	gene expression	CREB1	cyclic AMP-responsive element-binding protein 1	0.79	S271	P16220

Fold change represents a ratio of STK25$^{-/-}$/STK25$^{+/+}$. Phosphorylation sites, description, and accession numbers for each uniprot ID are listed. All changes met a significance threshold of a false discovery rate (FDR)-corrected q value <0.05.

KEY RESOURCES TABLE

REAGENT or RESOURCE	SOURCE	IDENTIFIER
Antibodies		
Anti-Flag Affinity Gel	Sigma-Aldrich	Cat# A2220, RRID:AB_10063035
Anti-V5 Agarose Affinity Gel	Sigma-Aldrich	Cat# A7345, RRID:AB_10062721
Anti-GAPDH	Cell Signaling Technology	Cat# 3683, RRID:AB_1642205
Anti-STK25	Abcam	Cat# ab157188, RRID:AB_2725788
Anti-Flag	Sigma-Aldrich	Cat# F3165, RRID:AB_259529
Anti-GM130	Cell Signaling Technology	Cat# 12480, RRID:AB_2797933
Anti-PRKAR1A	Abcam	Cat# ab139695, RRID:AB_2893184
Anti-pS77 PRKAR1A	Abcam	Cat#ab139682, RRID:AB_2904566
Anti-pS83 PRKAR1A	Abcam	Cat#ab154851, RRID:AB_2904567
Anti-PRKAR2A	Protein Tech	Cat# 10142-2-AP, RRID:AB_2922955
Anti-TnI	Cell Signaling	Cat# 4002, RRID:AB_2206278
Anti-TnI-pS23/S24	Cell Signaling	Cat# 4004, RRID:AB_2206275
Anti-Phospholamban	Cell Signaling Technology	Cat# 14562, RRID:AB_2798511
Anti-Phospholamban-pS16/T17	Cell Signaling Technology	Cat# 8496, RRID:AB_10949102
Anti-Ryanodine Receptor 2	Abcam	Cat#ab196355, RRID:AB_2904568
Anti-Ryanodine Receptor 2-pS2808	Abcam	Cat# ab59225, RRID:AB_946327
Anti-V5	Sigma-Aldrich	Cat# V8137, RRID:AB_261889
Anti-PKA Catalytic subunit	Abcam	Cat# ab26322, RRID:AB_2170049
Anti-mouse IgG (HRP conjugated)	Cell Signaling Technology	Cat# 7076, RRID:AB_330924
Anti-rabbit IgG (HRP conjugated)	Cell Signaling Technology	Cat# 7074, RRID:AB_2099233
Anti-CD172a/b	Biolegend	Cat# 323805; RRID:AB_830704
Anti-CD90	Invitrogen	11-0909-42, RRID:AB_10668828
Anti-TNNT2	BD Biosciences	Cat# 565744, RRID:AB_2739341
Biological samples		
Human myocardial samples (IRB#AAAR0055)	National Disease Research Interchange (https://ndriresource.org/ats)	N/A
Chemicals, peptides, and recombinant proteins		
Y-27632 dihydrochloride	Tocris	Cat# 1254
CHIR 99021	Tocris	Cat# 4423
Wnt-C59	Tocris	Cat# 5148
Forskolin	Sigma-Aldrich	Cat# F6886
Lipofectamine 3000	invitrogen	Cat# L3000015
Fast SYBR Green mixture	Life Technologies	Cat# 4385612
Recombinant protein STK25	ORIGENE	Cat# TP303215
Recombinant protein PRKAR1A	Abnova	Cat# H00005573_P01
In vitro kinase buffer	Cell Signaling	Cat# 9802

REAGENT or RESOURCE	SOURCE	IDENTIFIER
Critical commercial assays		
PKA activity kit	Invitrogen	Cat# EIAPKA
10-plex TMT kit	Navarrete-Perea et al. (2018)	PMID: 29734811
SmartSeq Ultra Low V4 kit	Clontech/Takara	R400752
Nextara XT Library Prep Kit	Illumina	FC-131-1024
RNeasy Mini kit	Qiagen	Cat#74004
On-column DNAse digestion	Qiagen	Cat# 79254
Superscript™ III First-Strand Synthesis SuperMix	Invitrogen	Cat# 18080400
Real Time Glo cell viability assay	Promega	Cat# G9712
Deposited data		
Sequencing of WT versus STK25KO cardiomyocytes	This paper	NCBI GEO: GSE195514
Proteomic data	This paper	PRIDE ProteomeXchange: PXD031367
Experimental models: Cell lines		
HEK293T	ATCC	Cat# CRL-3216, RRID:CVCL_0063
HiPSC (WTC cell line)	Material Transfer Agreements from Bruce Conklin, Gladstone Institute	N/A
Experimental models: Organisms/strains		
C57BL/6J mice (AABC1503)	The Jackson Laboratory	Strain #000664
Oligonucleotides		
On-TargetPlus siRNA targeting STK25	Horizon Discovery	Cat# L-004873-00-0050
ON-TARGETplus non-targeting pool	Horizon Discovery	Cat# D-001810-10-50
MISSION esiRNA targeting PRKAR1A	Sigma-Aldrich	Cat# EHU071341
Fwd Primer for STK25: GCTCCTACCTAAAGAGCACCA	IDT	N/A
Rev Primer for STK25: TGGCAATGTATGTCTCCTCCAG	IDT	N/A
Fwd Primer for GAPDH: GGACTCATGACCACAGTCCATG	IDT	N/A
Rev Primer for GAPDH: CAGGGATGATGTTCTGGAGAGC	IDT	N/A
Recombinant DNA		
CRISPR-Cas9 gRNA for STK25 knockout in iPSC	ORIGENE	Cat# KN203215G
CRISPR-Cas9 gRNA for STK25 knockout in mice	Synthego	Cat# sgRNA-stk25-7367, Cat# sgRNA-stk25-td10150
Flag-Empty Vector control	GeneCopoeia	Cat# EX-NEG-M46
Flag-WT-STK25 vector	GeneCopoeia	Cat# EX-M0142-M46
Flag-K49R/T147A-STK25 vector	Vector Builder	N/A
V5-PRKAR1A	Vector Builder	VB200124-1141aes
V5-S77A/S83A-PRKAR1A	Vector Builder	VB200124-1126jtp
V5-S77E/S83E-PRKAR1A	Vector Builder	VB200124-1127pst
Software and algorithms		
Real-Time Analysis Illumina	Illumina	https://www.illumina.com/informatics/sequencing-data-analysis.html

REAGENT or RESOURCE	SOURCE	IDENTIFIER
Bcl2fastq 2.19	Illumina	https://support.illumina.com/sequencing/sequencing_software/bcl2fastq-conversion-software.html
Kallisto 0.44.0	Bray et al. (2016)	https://pachterlab.github.io/kallisto/
DESeq2 1.28.1	Love et al. (2014)	https://bioconductor.org/packages/release/bioc/html/DESeq2.html
GSEA 4.10.0	Subramanian et al. (2005)	https://www.gsea-msigdb.org/gsea/index.jsp